ISABE-2009-02

INVESTIGATION OF UNSTEADY FLOW BEHAVIOR IN TRANSONIC COMPRESSOR ROTORS WITH LES AND PIV MEASUREMENTS

Chunill HAH[1], Melanie VOGES[2], Martin MUELLER [3] and Heinz-Peter SCHIFFER[3]

[1]NASA Glenn Research Center,
MS 5-11, Cleveland, Ohio 44135

[2]German Aerospace Center (DLR)
D-51147 Koeln, Germany

[3]Technische Universität Darmstadt
D-64287 Darmstadt, Germany

ABSTRACT

In the present study, unsteady flow behavior in a modern transonic axial compressor rotor is studied in detail with large eddy simulation (LES) and particle image velocimetry (PIV). The main purpose of the study is to advance the current understanding of the flow field near the blade tip in an axial transonic compressor rotor near the stall and peak-efficiency conditions. Flow interaction between the tip leakage vortex and the passage shock is inherently unsteady in a transonic compressor. Casing-mounted unsteady pressure transducers have been widely applied to investigate steady and unsteady flow behavior near the casing. Although many aspects of flow have been revealed, flow structures below the casing cannot be studied with casing-mounted pressure transducers. In the present study, unsteady velocity fields are measured with a PIV system and the measured unsteady flow fields are compared with LES simulations. The currently applied PIV measurements indicate that the flow near the tip region is not steady even at the design condition. This self-induced unsteadiness increases significantly as the compressor rotor operates near the stall condition. Measured data from PIV show that the tip clearance vortex oscillates substantially near stall. The calculated unsteady characteristics of the flow from LES agree well with the PIV measurements. Calculated unsteady flow fields show that the formation of the tip clearance vortex is intermittent and the concept of vortex breakdown from steady flow analysis does not seem to apply in the current flow field. Fluid with low momentum near the pressure side of the blade close to the leading edge periodically spills over into the adjacent blade passage. The present study indicates that stall inception is heavily dependent on unsteady behavior of the flow field near the leading edge of the blade tip section for the present transonic compressor rotor.

INTRODUCTION

In modern transonic compressors, flow near the rotor tip significantly influences the aerodynamic operation. A large fraction of the aerodynamic loss across a blade passage occurs near the casing, and it is believed that the compressor stall limit is determined by flow characteristics in the endwall region. The flow field near the compressor casing is very complex. Dominant features of the compressor endwall flow include the tip clearance flow; interactions among the tip clearance flow, the passage shock, and the endwall boundary layers; and accumulation of low momentum fluid due to radial migration.

Tip clearance flow in compressors has been widely studied (for example Hah [1988], Copenhaver et al. [1996], Storor [1991], Chima [1998], Hah and Loellbach [1999], Suder and Celestina [1994], Van Zante et al. [2000]). Tip clearance flow arises due to the pressure difference between the pressure and suction sides of the blade in the tip gap area. Flow through the tip gap interacts with the incoming passage flow near the suction side of the blade as it leaves the blade tip section, forming the tip clearance vortex. The vortex core is formed by fluid originating from the leading edge of the blade. Fluid flowing over the remainder of the blade rolls around this core vortex and adds swirl intensity. Some tip clearance flow originating near the casing travels over to the tip gap of the adjacent blade, resulting in so called double leakage flow (Smith [1993]). Near the stall condition, the pressure difference across the blade tip section increases and the interaction between the tip clearance flow and the passage flow becomes stronger. This causes more mixing losses and an increase in aerodynamic blockage near the casing. In some subsonic compressor rotors, the core vortex encounters a stagnation point formed by the reversed clearance flow, and vortex breakdown can occur (Furukawa et al. [1999], Maerz et al. [2002]).

In transonic rotors, strong interaction between the tip clearance vortex and the blade passage shock is expected when the rotor operates near stall. Various recent studies (for example, Schlechtriem and Loetzerich [1997], Hoffmann and Ballmann [2003], and Yamada et al. [2003]) have proposed tip vortex breakdown as a possible cause of stall inception in transonic compressor rotors. Vortex breakdown is defined as a phenomenon in which an abrupt change in the vortex core structure occurs. In transonic compressors, it is argued that passage shock/tip clearance vortex interaction can cause such vortex breakdown.

Although great advances have been made in flow measurement technology in turbomachinery over the last decade, it has not been possible to measure unsteady velocity fields near the rotor tip area. The most useful unsteady flow measurements have been obtained through casing-mounted unsteady pressure transducers. To understand endwall flow structures adequately, the unsteady velocity field below the casing should be measured with acceptable accuracy. Most previous analytical studies of tip clearance flow have been based on the assumption of steady flow. The pressure field near the rotor tip, however, becomes transient at near-stall operation. Consequently the tip clearance vortex becomes transient too. Therefore, unsteady characteristics of tip clearance flow and its interaction with the passage shock should be properly investigated. In the present study, the unsteady flow field near the rotor tip in a modern transonic compressor rotor is investigated with PIV measurement. The measured transient flow fields are compared with simulation results from LES.

TEST ROTOR AND TEST FACILITY

Figure 1 shows an overview of the test stand at the Department of Gas Turbine and Aerospace Propulsion at the Technical University of Darmstadt, Germany. The compressor stage under investigation in this study is the front stage of a high-pressure compressor in a modern commercial turbofan. Ambient air is led through a settling chamber and a bellmouth before entering the compressor stage. The rotor is driven by an 800 KW DC-drive and the shaft speed and power are measured by a torquemeter. Details of instrumentation, post-processing and measurement uncertainties are given by Bergner and Henneke [2003]. Since the volume between the stage and the throttle is small compared to the inlet duct length, rotating stall is considered to be the dominant mode of instability.

The investigated transonic rotor is the baseline geometry, designed with radially stacked CDA profiles. Figure 2 shows a front view of the rotor with the full-annulus grid. The measured tip gap at design speed is 1.55 mm, 0.95% of the mean blade span. The design parameters of the tested rotor are given in Table 1.

For the current investigation, the compressor test rig was modified for PIV measurement. Figure 3 shows laser light sheet positions in relation to the blade height and compressor casing. Steady and unsteady PIV investigation was performed at four operating points. In the present study, PIV data at 95% rotor height are used to compare with LES results. Figure 4 shows radial light sheet positions. Details of the PIV setups and uncertainty of the measurement are given by Voges et al. [2008].

NUMERICAL PROCEDURE

A Large Eddy Simulation (LES) method was applied in the present study to accurately capture unsteady interactions between the tip clearance vortex and the passage shock. With spatially-filtered Navier-Stokes equations, the subgrid-scale stress tensor term must be modeled properly for closure of the governing equations. A Smagorinsky-type eddy-viscosity model was used for the subgrid stress tensor, and the standard dynamic model by Germano et al. [1991] was applied.

In the current study, the governing equations are solved with a pressure-based implicit method using a fully conservative control volume approach. A third-order accurate interpolation scheme is used for the discretization of convection terms and central differencing is used for the diffusion terms. The method is of second-order accuracy with smoothly varying grids. For the time-dependent terms, an implicit second-order scheme is used and a number of sub-iterations are performed at each time step. Details of the numerical method and applications to transonic flows are given by Hah and Wennerstrom [1991].

The inflow boundary of the computational domain was located 6 average blade heights upstream of the rotor leading edge in order to damp out any possible reflections. Likewise, the outflow boundary was located six blade heights downstream from the trailing edge. The computational grid for a single blade passage consists of 198 nodes in the blade-to-blade direction, 128 nodes in the spanwise direction, and 560 nodes in the streamwise direction. The rotor tip clearance geometry is accurately represented by 28 nodes in the blade-to-blade direction, 16 nodes in the spanwise direction, and 140 nodes in the streamwise direction. The I-grid topology is used to reduce grid skewness and a single-block grid is used. All the computations were performed with NASA's Columbia supercomputer system, which allows parallel computation with up to 512 processors.

Standard boundary conditions for an isolated rotor were applied at the boundaries of the computational domain. Circumferentially averaged static pressure at the casing was specified to control the mass flow rate. Non-reflecting boundary conditions were applied at the inlet and the exit boundaries.

OVERALL FLOW STRUCTURE

Measured and calculated pressure rise characteristics of the rotor at the design rotor speed are shown in Fig. 5. Both the PIV measurement and LES analysis were conducted at the design condition and near stall. All the numerical simulations were performed for the isolated rotor configuration. The current compressor stage has a relatively large space between the rotor and the stator. Therefore, upstream influence of the stator was not included in the numerical simulations. The current study is focused on

investigating unsteady flow behavior near the tip region before stall inception occurs. Therefore a single-blade-passage analysis with periodicity conditions was performed.

Figure 6 shows comparisons of measured and calculated endwall static pressure distributions at the design and near-stall conditions. The time-averaged LES solution shown in Fig. 6 was obtained by averaging instantaneous solutions over 2000 time steps. The overall measured flow structures at both operating conditions are well reproduced by the LES computation. The measured static pressure distribution shows a low-pressure area immediately downstream of the tip clearance vortex/passage shock interaction. The time averaged distribution from the LES also shows this area clearly, which indicates that the current LES simulates the interaction between the tip clearance vortex and the passage shock realistically. Measured and calculated pressure distributions near peak efficiency show that the tip clearance core vortex travels further downstream after it encounters the passage shock. Near stall, on the other hand, the clearance vortex disappears as it meets the passage shock. As is well known, interaction between the tip leakage vortex and the passage shock becomes significant and the flow becomes highly oscillatory as the rotor operates near stall.

TIP CLERANCE FLOW AT PEAK EFFICIENCY FROM PIV AND LES

Figure 7 shows calculated instantaneous endwall pressure distributions at three different time steps at the peak efficiency operating condition. These results show that the pressure distribution on the casing does not change significantly with time. Nor does the tip clearance vortex core move noticeably. The flow field immediately after tip vortex/shock interaction changes slightly with time. The tip clearance vortex does not break down even after it interacts with the passage shock. Overall the flow field is fairly steady when the rotor operates at peak efficiency.

Changes in velocity vectors near the leading edge at three different times are given in Fig. 8. These results indicate that velocity vectors near the leading edge behind the shock are not steady. Also, some kind of vortex shedding occurs around the leading edge.

Measured contours of velocity magnitude near the leading edge at two different times are shown in Fig. 9. These contours show that flow field behind the shock is unsteady, and changes in flow incidence are evident. Downstream movement of the low-velocity area near the suction surface is observed.

Figure 10 shows changes in calculated contours of velocity magnitude near the leading edge. The measured values in Fig. 9 are on the flat plane of the laser beam while the calculated values in Fig. 10 are on the curved surface of 95% blade span. The calculated contours of the velocity magnitude clearly show movement of the low-velocity area on the blade suction side.

The calculated instantaneous distributions of static pressure and velocity magnitude shown in Figures 8 and 10 indicate that the tip clearance vortex does not break down even as it goes through the passage shock at this operating condition.

Both the PIV and LES results show that the overall flow field is almost steady near the peak efficiency condition. However, interaction between the tip clearance vortex and the passage shock is unsteady and some vortex shedding occurs near the leading edge behind the shock system.

TIP CLEARANCE FLOW NEAR STALL FROM PIV AND LES

Calculated instantaneous endwall pressure distributions near stall operation are given in Fig. 11. Compared to the pressure distribution near peak efficiency, the tip clearance core vortex forms further away from the suction surface as the pressure difference across the blade becomes larger. The calculated instantaneous casing pressure distributions also indicate that the tip leakage vortex oscillates significantly.

Measured and calculated instantaneous axial velocity contours are shown in Figs. 12 and 13. Calculated axial velocity contours are in reasonable agreement with the measured PIV data. The operating condition of the PIV measurements seems to be further toward stall inception than that of the LES calculation. Measured instantaneous axial velocity contours in Fig. 12 show that the tip clearance vortex oscillates substantially. The vortex core oscillates in the axial direction by as much as 10% of the axial blade chord. Calculated instantaneous axial velocity contours show that vortex shedding occurs at the leading edge behind the shock front. The shed vortex travels from the suction surface to the pressure surface with a frequency that is non-synchronous with the rotor. The flow field after the passage shock is highly unsteady according the results shown in Fig. 13.

Calculated instantaneous velocity vectors near the leading edge are shown in Fig. 14. At this operating condition, the passage shock is completely detached from the blade and the flow incidence near the leading edge changes almost 20 degrees in time. This change in flow incidence is the direct cause of the vortex shedding at the leading edge. The PIV measurements shown in Figs. 9 and 12 also prove that the flow field behind the shock is highly unsteady.

Bergner et al. [2006] measured changes in pressure difference across the blade near the leading edge near stall. Figure 15 shows the frequency of the measured pressure differences from that study as a function of magnitude. The measured pressure differences in Figure 15 imply that the flow incidence changes substantially. Both the measured instantaneous velocity fields from PIV and the measured pressure difference across the blade tip support the transient characteristics of the calculated flow.

The frequency distribution of calculated pressure differences across the blade tip from the current study is shown in Fig. 16. These results agree well with the unsteady pressure measurements in Fig. 15. The calculated instantaneous pressure and velocity fields in Figs. 13 and 16 clearly show that the tip clearance core vortex is intermittent

and it does not maintain its shape when it interacts with the passage shock. The calculated instantaneous velocity vectors indicate that some flow intermittently spills over into the next blade passage around the leading edge. Also, the tip clearance core vortex stays well inside the blade passage and does not move forward even as stall inception occurs. These calculated transient flow phenomena near the leading edge are supported by the unsteady endwall pressure measurements as well as the unsteady PIV data.

CONCLUDING REMARKS

The unsteady flow behavior near the casing in a transonic compressor rotor was investigated in detail with LES calculations and PIV measurements. The flow fields from the LES simulation show that the formation of the tip clearance vortex is intermittent. Fluid intermittently spills around the leading edge into the adjacent blade passage at operation near stall. The calculated unsteady flow phenomena near the leading edge of the rotor tip are confirmed by the PIV measurements as well as unsteady pressure measurements at the endwall. The phenomena of flow instability and stall inception in a transonic compressor are directly related to the observed unsteady flow behavior near the casing. Further studies are required to make quantitative validation of the calculated unsteady flow fields. Both the PIV measurements and the unsteady pressure measurements on the compressor casing should be used together to validate the numerical simulation.

REFERENCES

Bergner, J. and Hennecke, D. K., 2003, "Experimental Study of Stall Inception of a Single-Stage Transonic Compressor," Proc. 16th Symposium on Air Breathing Engines, ISABE-2003-1081.

Chima, R. V., 1998, "Calculation of Tip Clearance Effects in a Transonic Compressor Rotor," ASME Journal of Turbomachinery, Vol. 120, pp. 131-139.

Copenhaver, W. W., Mayhew, E. R., Hah, C., and Wadia, A. R., 1996, "The Effects of Tip Clearance on a Swept Transonic Compressor Rotor," ASME Journal of Turbomachinery, Vol. 118, pp. 230-239.

Furukawa, M., Inoue, M., Kuroumaru, M., Saiki, K., and Yamada, K., 1999, "A Role of Tip Leakage Vortex Breakdown in Compressor Rotor Aerodynamics," ASME Journal of Turbomachinery, Vol. 121, pp. 469-480.

Germano, M., Piomelli, U., Moin, P., and Cabot, W. H., 1991, "A Dynamic Subgrid-Scale Eddy-Viscosity Model," Journal of Fluid Mechanics, Vol. A3, pp. 170-176.

Hah, C, and Loellbach, J., 1999, "Development of Hub Corner Stall and its Influence on the Performance of Axial Compressor Blade Rows," ASME Journal of Turbomachinery, Vol. 121, No. 1, pp. 67-77.

Hah, C., 1986, "A Numerical Modeling of Endwall and Tip Clearance Flow of an Isolated Compressor," ASME Journal of Engineering for Gas Turbines and Power, Vol. 108, No. 1, pp. 15-21.

Hah, C. and Wennerstrom, A. J., 1991, "Three-Dimensional Flow Fields Inside a Transonic Compressor with Swept Blades," ASME Journal of Turbomachinery, Vol. 113, No. 1, pp. 241-251.

Hoffman, W. H. and Ballman, J., 2003, "Some Aspects of Tip Vortex Behavior in a Transonic Turbocompressor," ISABE Paper 2003-1223.

Maerz, J., Hah, C., and Neise, W, 2002, "An Experimental and Numerical Investigation into the Mechanism of Rotating Instability," ASME Journal of Turbomachinery, Vol. 124, pp. 367-375.

Schlechtriem, S. and Loetzerich, M., 1997, "Breakdown of Tip Leakage Vortices in Compressors at Flow Conditions Close to Stall," ASME Paper 97-GT-41.

Smith L. H. Jr., 1993, Private communication.

Storer, J. A., 1991, "Tip Clearance Flow in Axial Compressors," Ph.D. Thesis, Cambridge University, United Kingdom.

Suder, K. L., and Celestina, M. L., 1994, "Experimental and Computational Investigation of the Tip Clearance Flow in a Transonic Axial Compressor Rotor," NASA TM-106711.

Voges, M, Schnell, R., Willert, C., and Moenig, R., 2008, "Investigation of Blade Tip Interaction with Casing Treatment in a Transonic Compressor".

Yamada, K, Furukawa, M., Inoue, M., and Funazaki, K., 2003, "Numerical Analysis of Tip Leakage Flow Field in a Transonic Axial Compressor Rotor," IGTC Paper 2003-095.

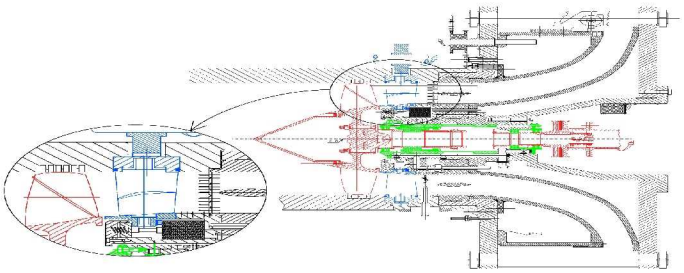

Figure 1: Cross section of test compressor stage.

Table 1: Rotor Design Parameters

Pressure ratio	1.5
Corrected mass flow rate	16.0 kg/s
Corrected tip speed	398 m/s
Inlet relative Mach number at tip	1.35
Inlet relative Mach number at hub	0.70
Shaft speed	20,000 rpm
Tip diameter	0.38 m
Rotor mean aspect ratio	0.94
Rotor solidity (hub/mid/tip)	1.9/1.5/1.2

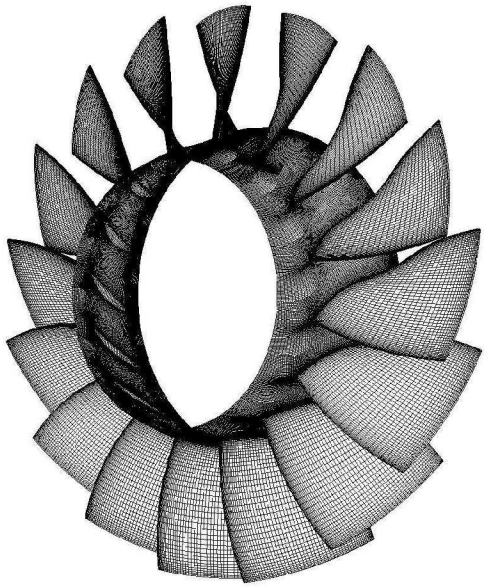

Figure 2: Front view of rotor full-annulus grid

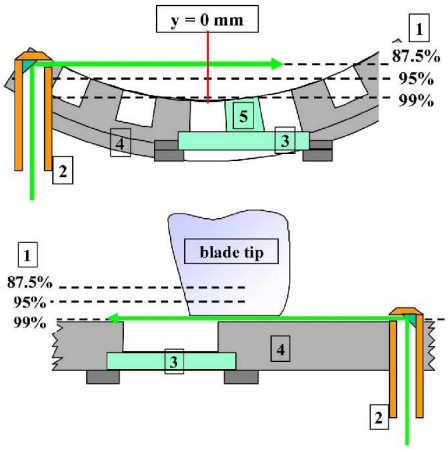

Figure 3: Laser light sheet positions in relation to the blade height.

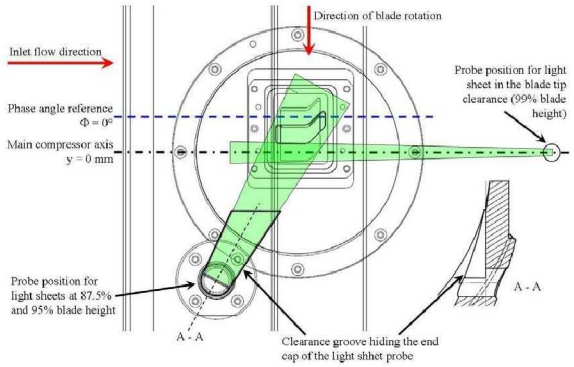

Figure 4: Window sheet and light sheet probe positions.

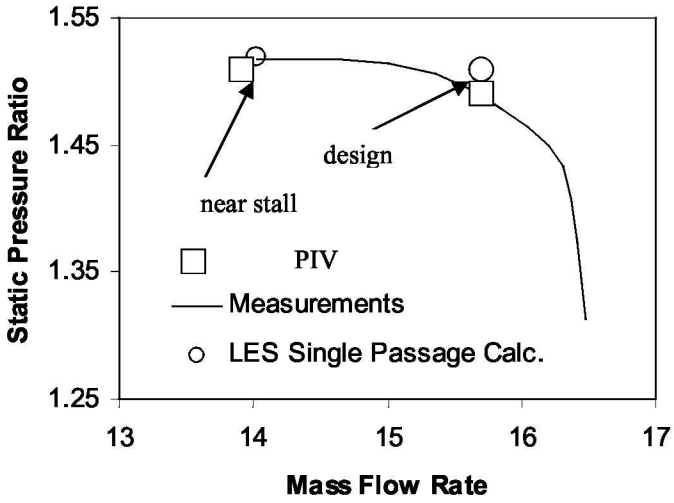

Figure 5: Pressure rise characteristics of the rotor.

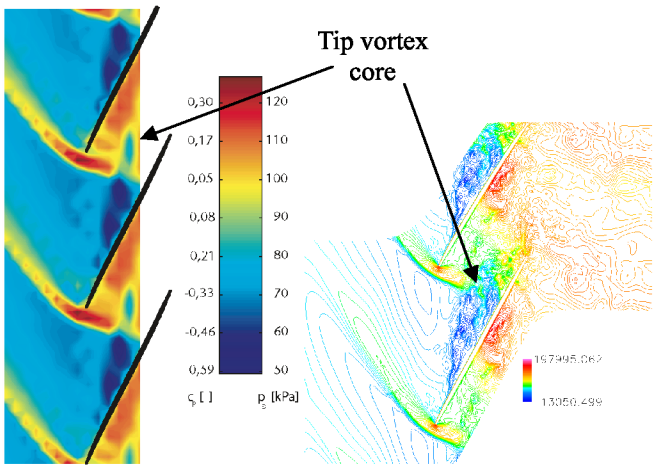

a) near peak efficiency.

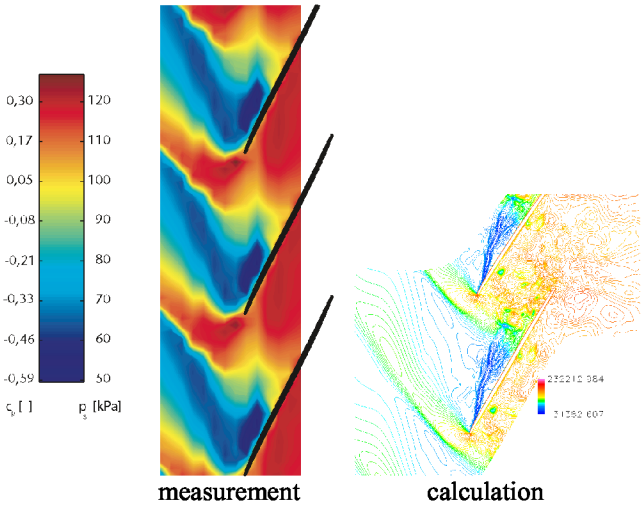

b) near stall

Figure 6: Comparison of measured and calculated casing static pressure distributions.

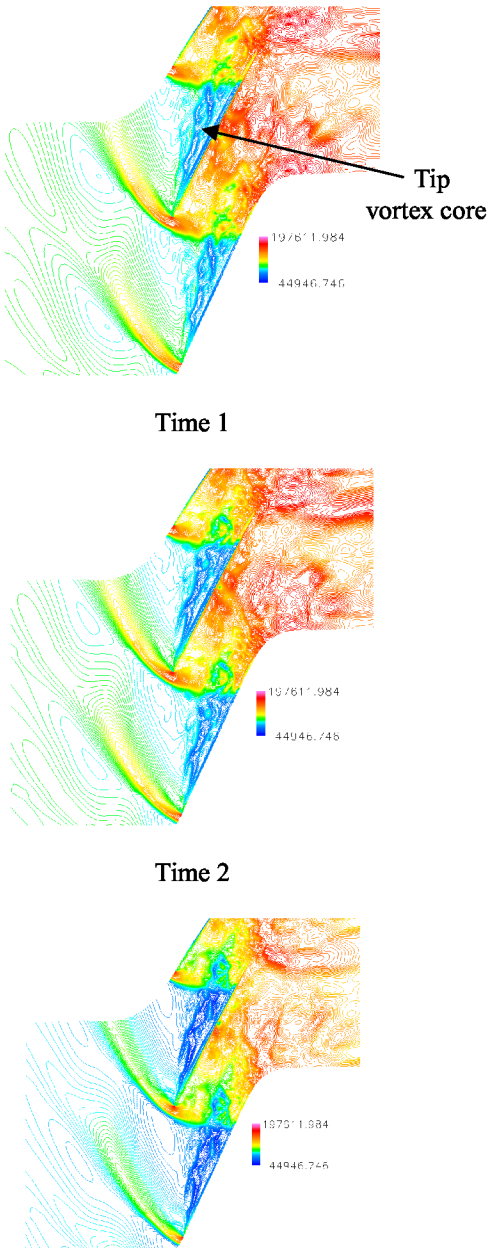

Figure 7: Calculated instantaneous casing pressure distribution near peak efficiency.

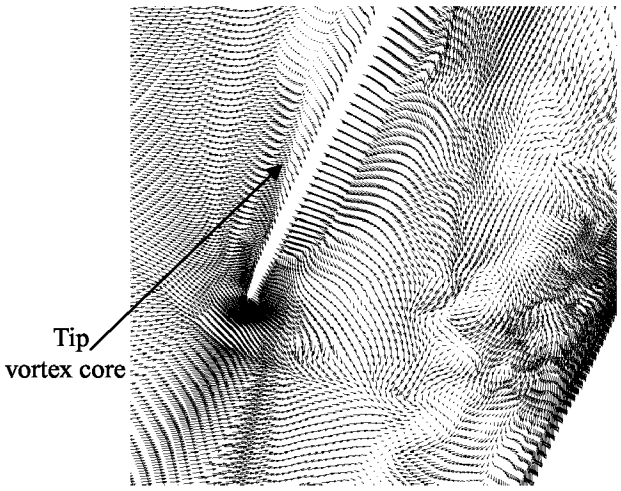

Time 1

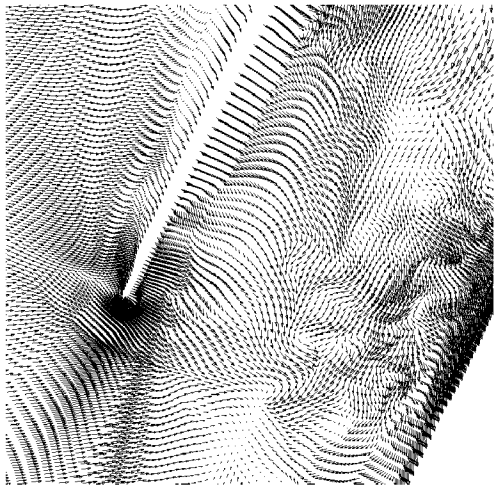

Time 2

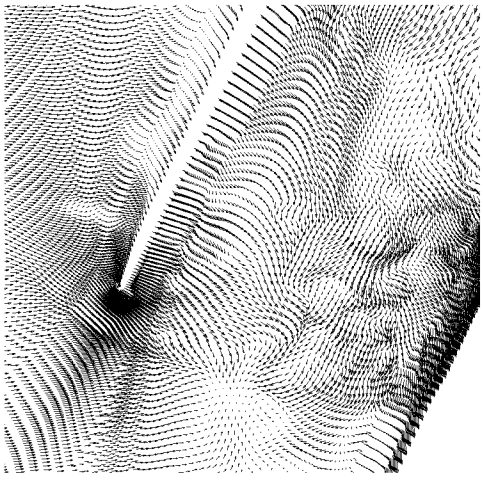

Time 3

Figure 8: Calculated instantaneous velocity vectors near peak efficiency.

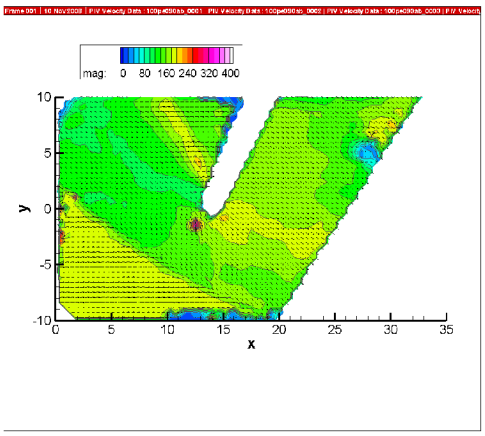

Time 1

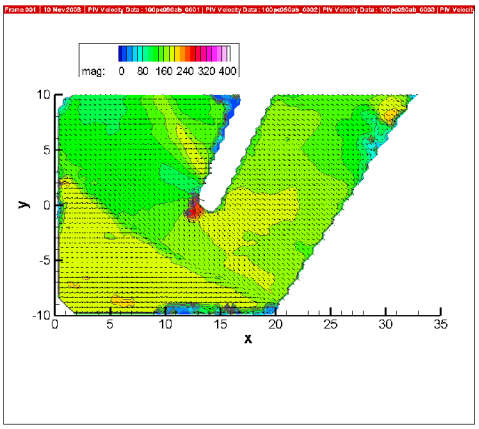

Time 2

Figure 9: Instantaneous magnitude of axial and tangential velocity components from PIV near peak efficiency.

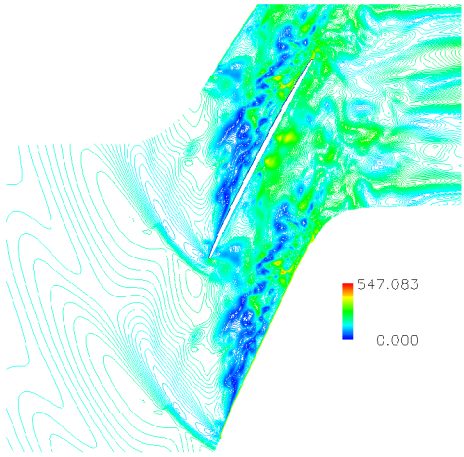

Time 1

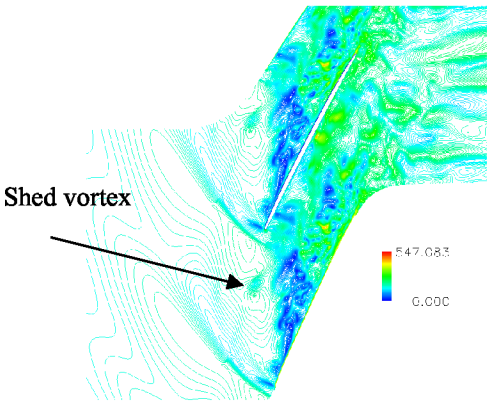

Time 2

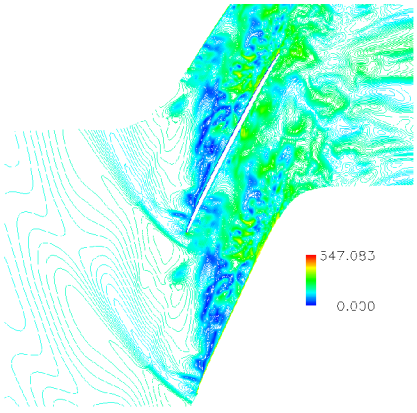

Time 3

Figure 10: Calculated instantaneous magnitude of total velocity near peak efficiency.

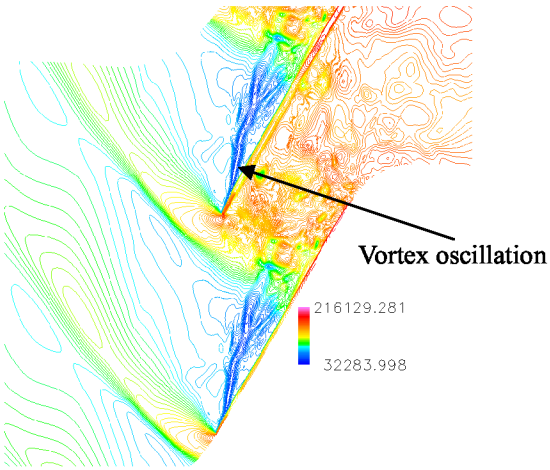

Time 1

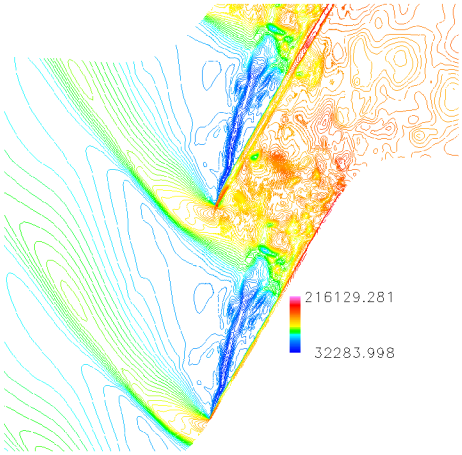

Time 2

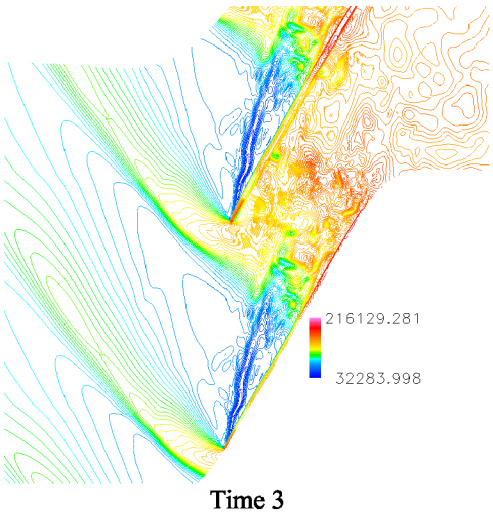

Time 3

Figure 11: Calculated instantaneous casing static pressure near stall.

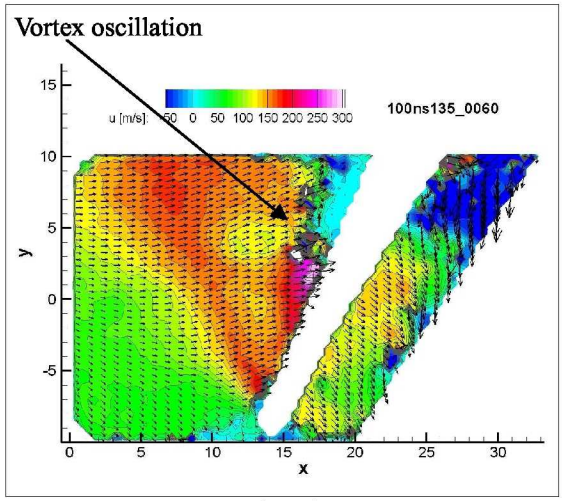

Time 1

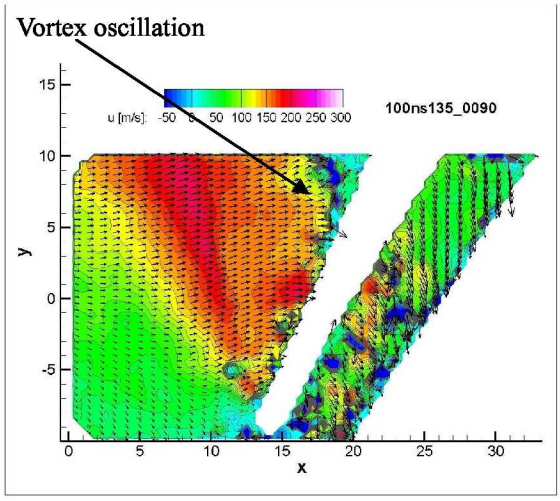

Time 2

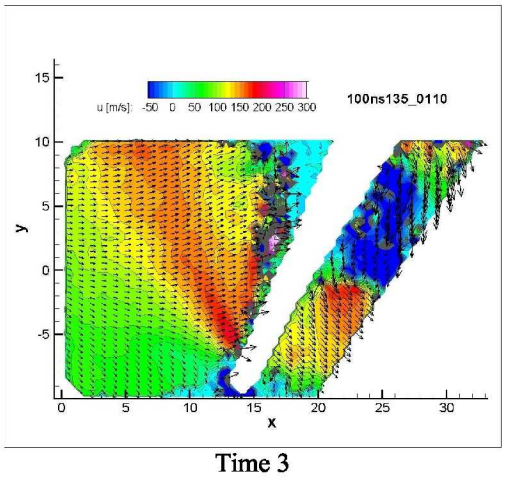

Time 3

Figure 12: Measured instantaneous axial velocity contours near stall.

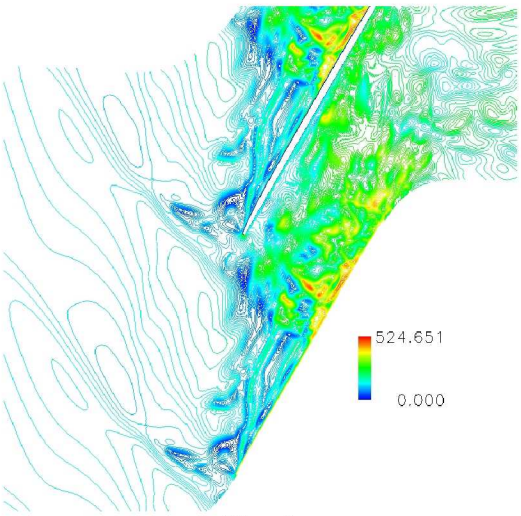

Time 1

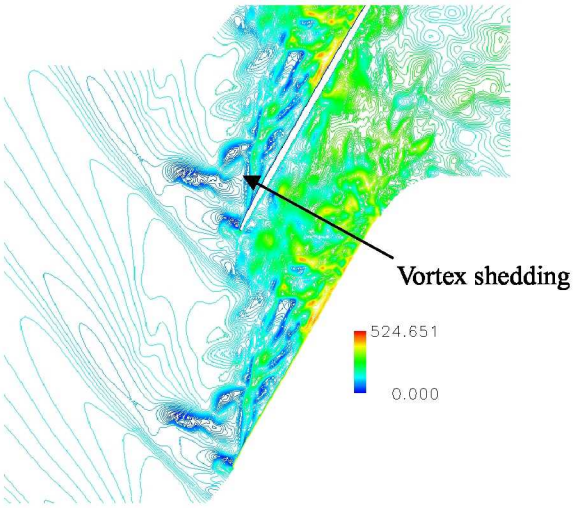

Time 2

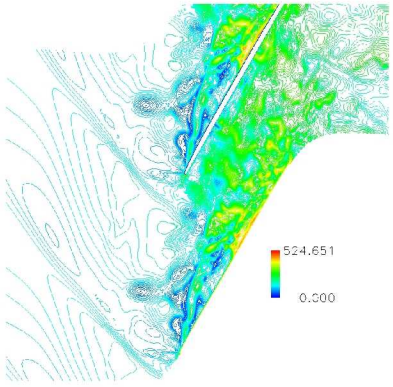

Time 3

Figure 13: Calculated instantaneous axial velocity contours, near stall.

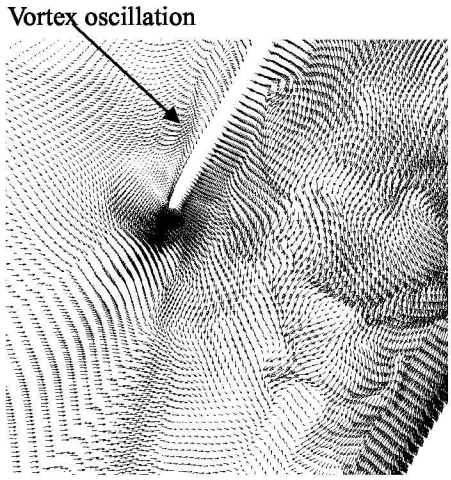

Time 1

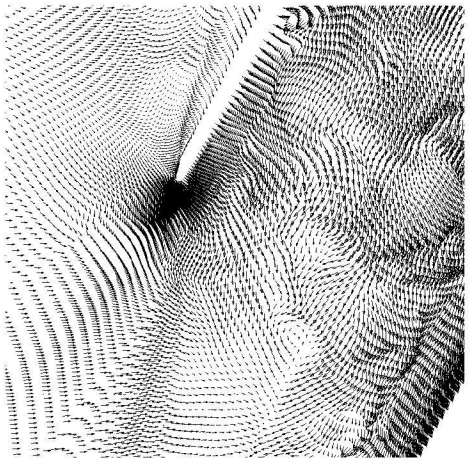

Time 2

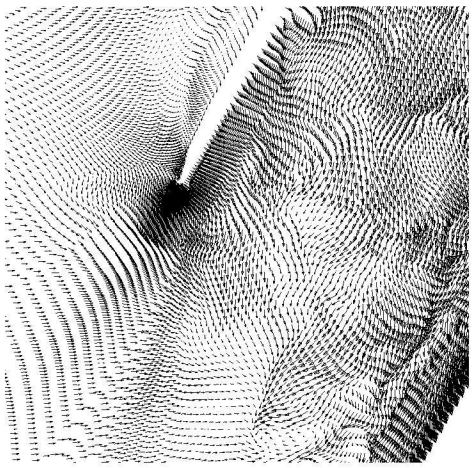

Time 3

Figure 14: Calculated instantaneous velocity vectors near stall.

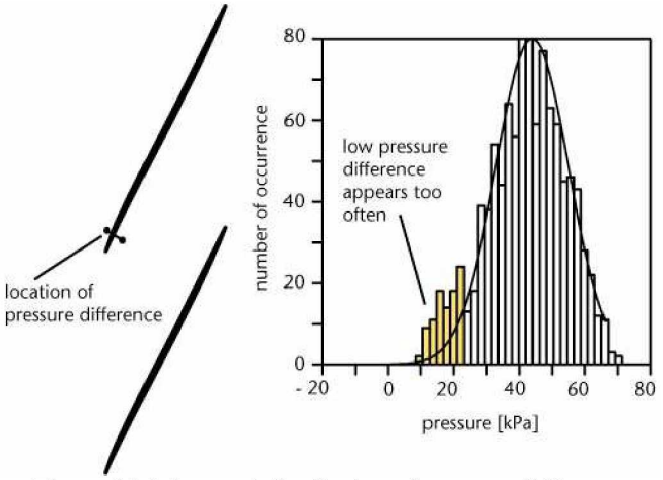

Figure 15: Measured distribution of pressure difference across blade tip near leading edge near stall.

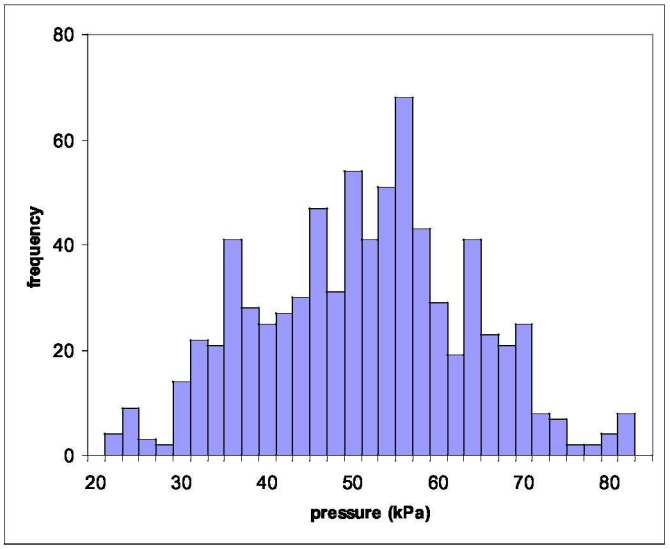

Figure 16: Calculated distribution of pressure difference across blade tip near leading edge near stall.